A valence tautomeric cobalt-dioxolene with an anchoring group for prospective chemical grafting to metal oxides

*Max Mörtel, Michael Seller, Frank W. Heinemann and Marat M. Khusniyarov**

Department of Chemistry and Pharmacy

Friedrich-Alexander University Erlangen-Nürnberg (FAU)

Egerlandstrasse 1, 91058 Erlangen

Germany

*corresponding author: marat.khusniyarov@fau.de

Electronic Supplementary Information

Table of Contents

General Experimental Methods 3
Synthesis 7
Crystallographic Data 8
Magnetic Properties 13
EPR Spectroscopy 18
Electronic Absorption Spectroscopy 21
Cyclic Voltammetry 25
Theoretical Calculations 29
References 30

General Experimental Methods

Materials. All starting materials and solvents were utilized as received without further purification unless otherwise noted. Pure anhydrous solvents were collected from a solid-state solvent purification system Glass Contour (Irvine, CA). Tetramer $[Co(^tBu\text{-dioxolene})_2]_4$,[1] ethyl-4-(1,10-phenanthrolin-6-yl)-benzoate **L**,[2] and reference complex $[Co(^tBu\text{-dioxolene})_2(phen)]$[3] (phen = 1,10-phenanthroline) were prepared according to literature methods with minor modifications (^{t}Bu-dioxolene – 3,5-di-*tert*-butyl-*o*-catecolate with undefined oxidation level).

Instrumentation. Elemental analyses were carried out with a EURO EA analyzer from EuroVector. Magnetic susceptibility data on solid samples were collected with a Quantum Design MPMS 3 Magnetometer. DC susceptibility data were collected in the temperature range 2 – 360 K on powder samples restrained within a polycarbonate gel capsule in the applied magnetic field of 0.1 T at 2 K min^{-1} heating/cooling rate and 5 K intervals. The magnetic susceptibility data were corrected for diamagnetism using an estimation $\chi_{m,\,diamag} = ½\, M_w \cdot 10^{-6}$ cm^{3}mol^{-1} with M_w being the molar mass of the compound.[4] Temperature-dependent χT product was fitted using the van't Hoff equation (1) to give the enthalpy and entropy changes ΔH and ΔS, respectively, for the *ls*-Co(III) → *hs*-Co(II) conversion, where χ_{LT} and χ_{HT} are low- and high-temperature limits for molar magnetic susceptibility, respectively, and TIP is temperature-independent paramagnetism.

$$\chi T = \frac{\chi_{LT} T + \chi_{HT} T e^{\frac{-\Delta H + T\Delta S}{RT}}}{1 + e^{\frac{-\Delta H + T\Delta S}{RT}}} + T \cdot TIP \qquad (1)$$

Field-dependent magnetization data were fitted using the Program PHI 3.1.5 by CHILTON *et al*.[5]

Variable-temperature NMR spectra were recorded with a JEOL ECP 400 MHz spectrometer in rotating 5 mm o.d. tubes and processed with *Delta V4.0* software provided by JEOL Ltd. All

solutions for electronic absorption spectroscopy were prepared under inert conditions and sealed in custom made Quartz SUPRASIL cells (QS). Room temperature spectra were recorded with a Shimadzu UV 3600 spectrophotometer. Variable-temperature electronic absorption spectra were recorded with an Analytik Jena SPECORD S600 spectrophotometer and fitted using the van't Hoff equation (2) to give the enthalpy and entropy changes ΔH and ΔS, respectively, for the *ls*-Co(III) $\rightarrow$ *hs*-Co(II)conversion, where A_{LT} and A_{HT} are low- and high-temperature limits for the absorbance.

$$A = \frac{A_{LT} + A_{HT} e^{\frac{-\Delta H + T\Delta S}{RT}}}{1 + e^{\frac{-\Delta H + T\Delta S}{RT}}} \qquad (2)$$

Electrochemical measurements were performed under nitrogen atmosphere at RT using a standard three-electrode setup with a Pt rotating disc electrode (RDE) as working and platinum rods as counter and reference electrodes. The potentiostat was a Metrohm μAutolab III/FRA2. Analyte solutions were prepared in CH_2Cl_2 containing 0.1 M $^{n}Bu_4NPF_6$ as supporting electrolyte and measured at room temperature. All potentials are referenced to the $Fc^{+/0}$ redox couple measured after adding ferrocene as internal standard to the analyte solution.

EPR spectra were recorded on a JEOL CW spectrometer JES-FA200 equipped with an X-band Gunn diode oscillator bridge, a cylindrical mode cavity, and N_2/He cryostat. The samples were measured in Quartz glass EPR tubes in solution (DCM, RT) or frozen solution (toluene, 93 K and 7 K).

Crystallographic Data. Crystals of **1** were obtained by slow vapor diffusion of Et_2O into a toluene solution of the complex and consisted of very thin black plates (see Figure S2). Colorless prisms

of **L** were obtained by a similar method using *n*-hexane and toluene. A suitable single crystal was embedded in protective perfluoropolyalkyether oil on a microscope slide and a single specimen was selected and subsequently transferred to the diffractometer. Intensity data for **1** were collected using MoK_α radiation (λ = 0.71073 Å) on a Bruker Kappa PHOTON II *IμS* Duo diffractometer equipped with QUAZAR focusing Montel optics at temperatures of 100 K and 293 K. Intensity data for **L** were collected using MoK_α radiation (λ = 0.71073 Å) on a Bruker Smart APEX II CCD area detector diffractometer with a Triumph curved graphite monochromator. Data were corrected for Lorentz and polarization effects, semi-empirical absorption corrections were performed on the basis of multiple scans using *SADABS*.[6] The structures were solved by direct methods (*SHELX XT*)[7] and refined by full-matrix least-squares procedures on F^2 using *SHELXL* 2018/3.[8] All non-hydrogen atoms were refined with anisotropic displacement parameters. In the crystal structure of **1 @ 293K** two of the *t*Bu groups were disordered. Two alternative orientations each were refined and resulted in site occupancies of 66.6(8) and 33.4(8) % for the atoms C12 – C14 and C12A – C14A, and of 75.2(8) and 24.8(8) % for the atoms C26 – C28 and C26A – C28A, respectively. Similarity and pseudo-isotropic restraints were applied to the anisotropic displacement parameters of the disordered atoms.

All hydrogen atoms were placed in positions of optimized geometry, their isotropic displacement parameters were tied to those of the corresponding carrier atoms by a factor of either 1.2 or 1.5. *Olex2* was used to prepare materials for publication.[9] Crystallographic data, data collection, and structure refinement details are given in Table S1.

Theoretical Calculations. The program ORCA 4.1.1 was used for all calculations.[10] Geometry optimizations were performed on truncated models with all *tert*-butyl and ethyl groups replaced by methyl groups, starting from the available X-ray structure. B3LYP[11, 12] functional was used.

We used def2-SVP and def2-TZVP basis sets[13] for C/H and non-C/H atoms, respectively, sped up with RIJCOSX approximation with def2/J auxiliary basis sets.[14] The *hs*-Co(II)(Cat^{2-})($SQ^{\bullet-}$) state was calculated as $S = 5/2$. Conductor-like polarizable continuum model (C-PCM)[15] was used while calculating electronic absorption spectra with TD-DFT. Molecular orbitals were visualized with Molekel.[16] Calculated electronic absorption spectra were produced with Chemcraft.[17]

Synthesis

[Co(^{t}Bu-dioxolene)$_2$L] (1)

Under inert atmosphere, ethyl-4-(1,10-phenanthrolin-6-yl)-benzoate (219 mg, 0.670 mmol) **(L)** dissolved in dry toluene (20 mL) was slowly added *via* cannula to a suspension of [Co(^{t}Bu-dioxolene)$_2$]$_4$ (336 mg, 0.168 mmol) in dry toluene (20 mL). The reaction was stirred for 1 h at 100 °C. Afterwards, the reaction mixture was cooled to RT and stirred for further 16 h before keeping at –25 °C overnight. Then, the suspension was filtered *via* cannula at –25 °C using an acetone/N_2 cooling bath. The solid was washed with dry toluene (5 mL) and dry *n*-hexane (3 x 5 mL). The filtrate was reduced in volume to ~1/2, stored at –25 °C overnight, the precipitate was filtered and washed. The combined solids were dried at 80 °C *in vacuo* to yield the product as a violet powder.

Yield: 0.260 mg (45 %);

Elemental analysis:

$CoC_{49}H_{56}N_2O_6$

calculated:	C: 71.09, H: 6.82, N: 3.38
found:	C: 70.72, H: 6.98, N: 3.39

Crystallographic Data

Crystallographic information: CCDC-2040229 (for **L @ 294K**), 2040230 (for **1 @ 100K**), and 2040231 (for **1 @ 293K**) contain the supplementary crystallographic data for compounds **L** and **1**, respectively, in this paper. The data can be obtained free of charge from The Cambridge Crystallographic Data Centre *via* www.ccdc.cam.ac.uk/structures.

Crystallographic data, data collection, and structure refinement details are given in Table S1.

Table S1: Crystallographic data, data collection, and refinement details.

	L @ 294K CCDC-2040229	**1 @ 100 K CCDC-2040230**	**1 @ 293 K CCDC-2040231**
Empirical formula	$C_{21}H_{16}N_2O_2$	$C_{49}H_{56}CoN_2O_6$	$C_{49}H_{56}CoN_2O_6$
Mol. Weight	328.36	827.88	827.88
Crystal shape, color	prisms, colourless	plate, black	plate, black
Crystal size [mm]	0.28 x 0.23 x 0.21	0.22 x 0.075 x 0.03	0.22 x 0.075 x 0.03
Temperature [K]	294	100	293
Crystal system	monoclinic	triclinic	triclinic
Space group	$P2_1/n$	$P\bar{1}$	$P\bar{1}$
a [Å]	10.9000(4)	10.64539(6)	10.8175(4)
b [Å]	10.3872(3)	11.6692(6)	11.9090(4)
c [Å]	15.0631(5)	17.9520(10)	17.9599(6)
α [°]	90	98.739(2)	99.162(1)
β [°]	102.886(2)	94.709(2)	93.243(1)
γ [°]	90	105.380(2)	105.816(1)
V [Å^3]	1662.5(1)	2109.3(2)	2185.50(13)
Z	4	2	2
ρ [g cm^{-3}] (calc.)	1.312	1.303	1.258
μ [mm^{-1}]	0.086	0.459	0.443
F (000)	688	878	878
T_{min};T_{max}	0.701; 0.746	0.667; 0.746	0.696; 0.746
2Θ interval [°]	5.4 ≤ 2 Θ ≤ 54.2	3.6 ≤ 2 Θ ≤ 54.2	3.9 ≤ 2 Θ ≤ 54.2
Coll. Refl.	29613	68512	82032
Indep. Refl.; R_{int}	3656, 0.032	9304, 0.081	9642, 0.077
Obs. refl. F_0 ≥4σ(F)	2518	7183	7064
No. ref. param.	227	536	598
wR_2 (all data)	0.136	0.1188	0.1424
R_1 (F_0 ≥4σ(F))	0.0475	0.0526	0.0594
GooF on F^2	1.075	1.059	1.063
$\Delta\rho_{max/min}$ [e Å^{-3}]	0.17; –0.25	0.62; –0.39	0.31; –0.26

Table S2: Comparison of selected bond distances of **1** at 100 and 293 K. The differences in bond lengths (Δ) are checked for significance (3σ).

	1 @ 100 K [Å]	**1 @ 293 K [Å]**	**$\Delta_{(293K–100K)}$ [Å]**	**3σ [Å]**[#]
Co–O1	1.9002(19)	1.910(2)	0.008	0.009
Co–O2	1.8857(18)	1.8907(19)	0.005	0.009
Co–O3	1.8793(18)	1.8857(19)	0.006	0.009
Co–O4	1.8567(18)	1.8605(28)	0.003	0.011
Co–N1	1.938(2)	1.944(2)	0.006	0.009
Co–N2	1.968(2)	1.975(2)	0.007	0.009

[#] $\sigma = (\sigma_A^2 + \sigma_B^2)^{1/2}$. $\Delta_{(293K–100K)}$ is significant if larger than 3σ.

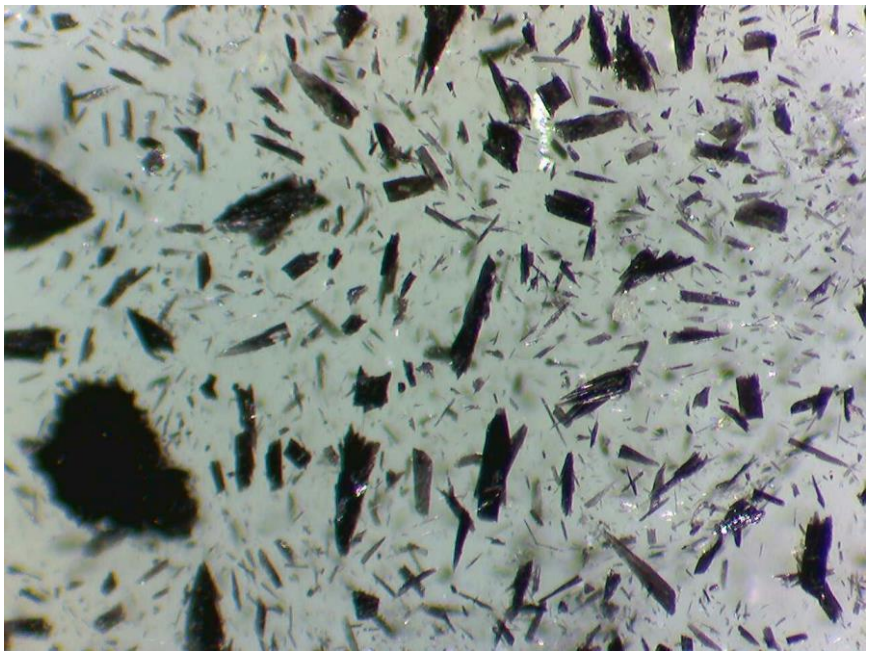

Figure S1: Microscope photograph of crystalline material of **1**.

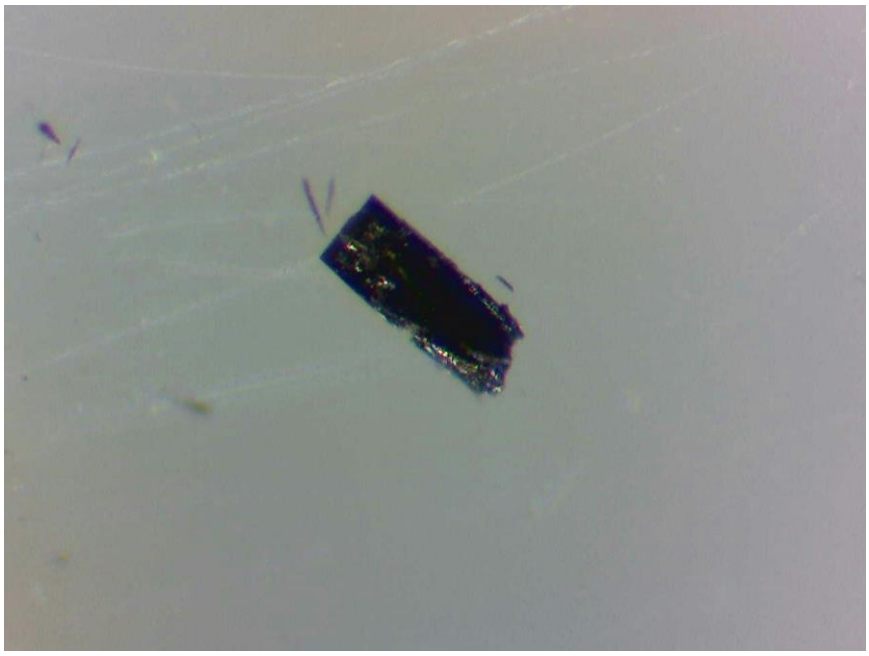

Figure S2: Microscope photograph of the crystalline sample of **1** used for structure determination.

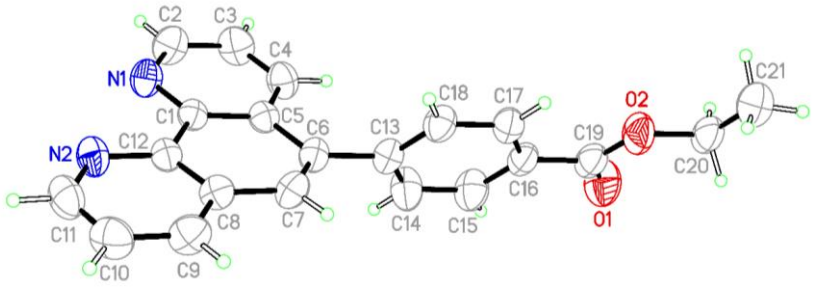

Figure S3: Solid-state molecular structure with applied numbering scheme of **L** @ 294 K. Thermal ellipsoids are drawn at the 50 % probability level.

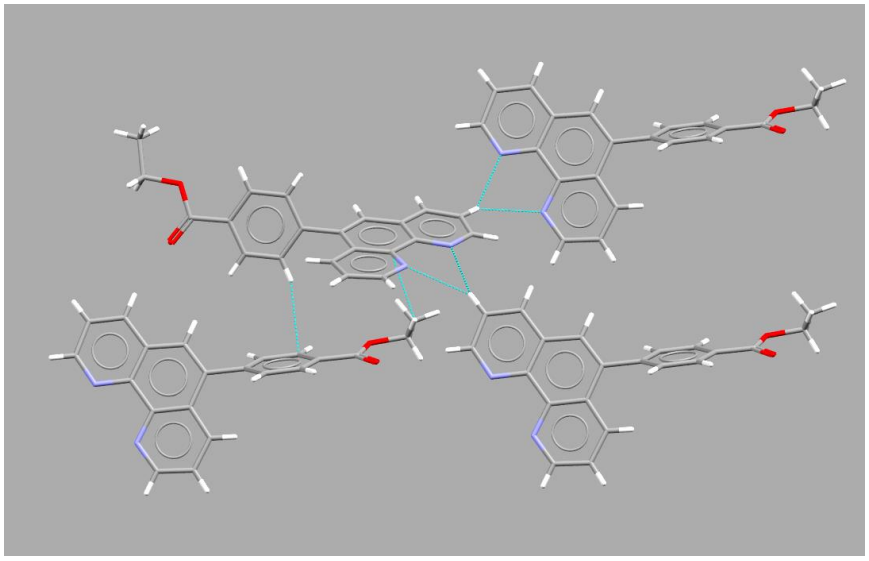

Figure S4: Short contacts between two molecules of **L** in the crystal structure (a half of the unit cell is shown).

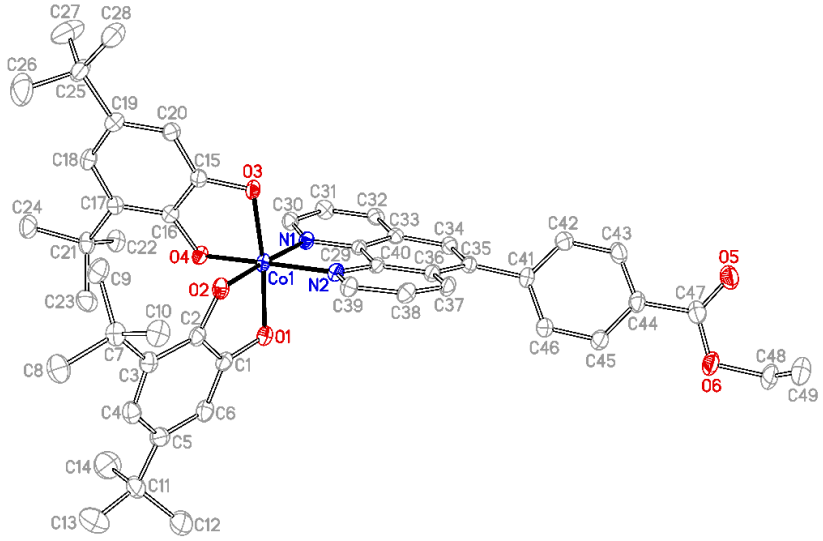

Figure S5: Solid-state molecular structure with applied numbering scheme of **1** @ 100 K. Thermal ellipsoids are drawn at the 50 % probability level. Hydrogen atoms are omitted for clarity.

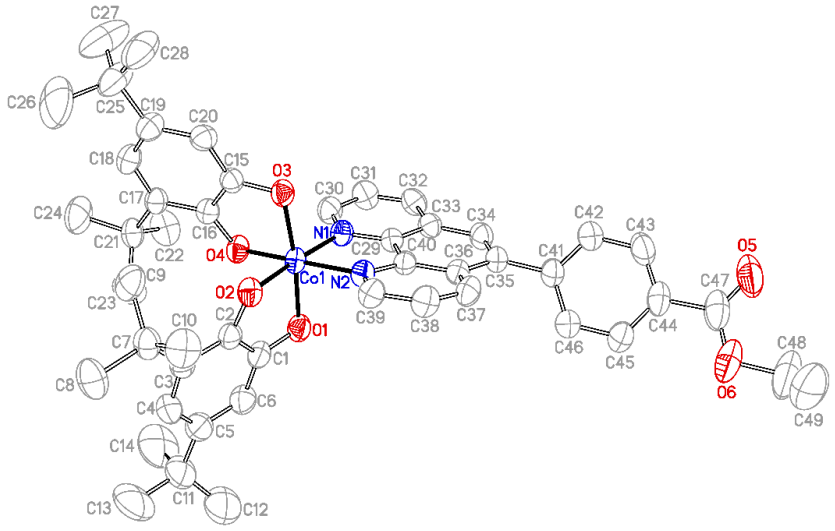

Figure S6: Solid-state molecular structure with applied numbering scheme of **1** @ 293 K. Thermal ellipsoids are drawn at the 50 % probability level. Hydrogen atoms are omitted for clarity.

Magnetic Properties

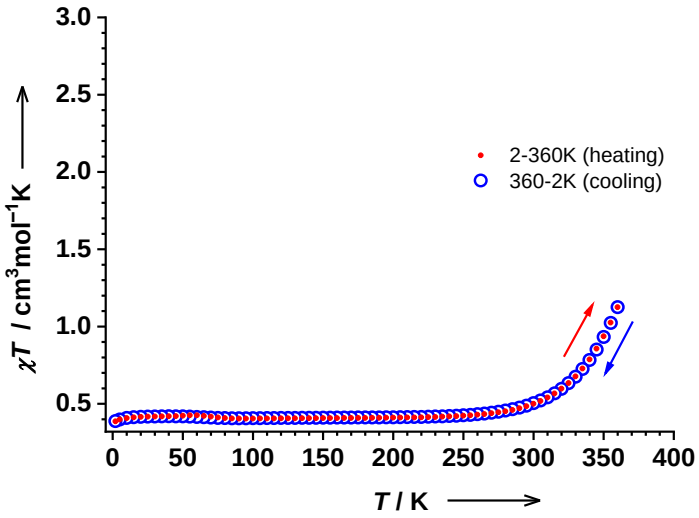

Figure S7: Variable temperature χT product of **1** measured on a powder sample at an external field of 0.1 T in the heating (red) and cooling (blue) mode (5 K steps, 2 K min^{-1}).

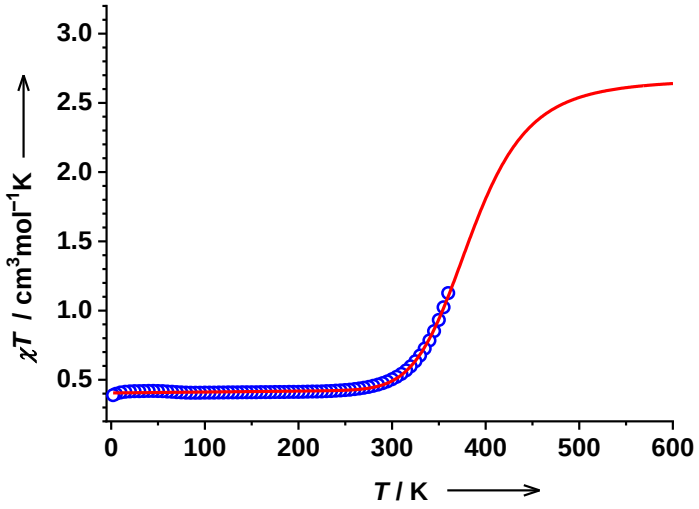

Figure S8: Variable temperature χT product of **1** measured on a powder sample at an external field of 0.1 T in the cooling mode (5 K steps, 2 K min^{-1}). Van't Hoff fit parameters: ΔH = 39.5(9) kJ mol^{-1}, ΔS = 103(3) J mol^{-1} K^{-1}, TIP = 6(1)·10^{-5} cm^3 mol^{-1}, and χT_{LT} = 0.405(2) cm^3 mol^{-1} K. The high temperature limit χT_{HT} is fixed at 2.625 cm^3 mol^{-1} K, assuming g_{Co} = 2.0 for the *hs*-Co^{II}(SQ)$_2$ state. The derived transition temperature is $T_{1/2} = \Delta H / \Delta S$ = 384 K.

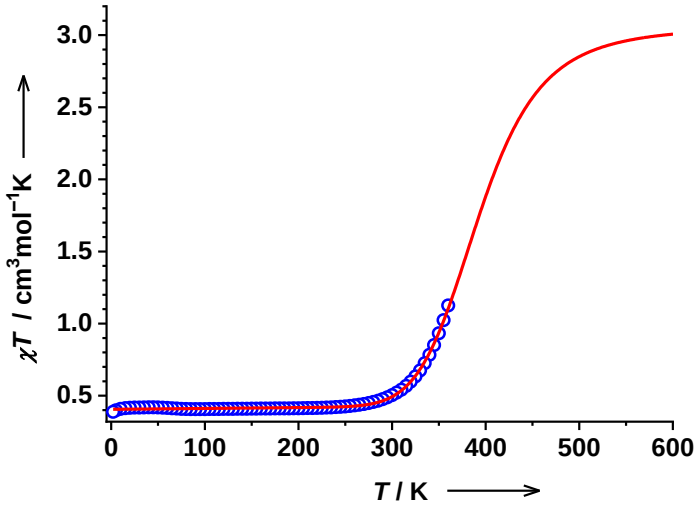

Figure S9: Variable temperature χT product of **1** measured on a powder sample at an external field of 0.1 T in the cooling mode (5 K steps, 2 K min^{-1}). Van't Hoff fit parameters: ΔH = 38.1(8) kJ mol^{-1}, ΔS = 97(2) J mol^{-1} K^{-1}, TIP = 6(1)·10^{-5} cm^3 mol^{-1}, and χT_{LT} = 0.406(2) cm^3 mol^{-1} K. The high temperature limit χT_{HT} is fixed at 3.015 cm^3 mol^{-1} K, assuming g_{Co} = 2.2 for the *hs*-Co^{II}(SQ)$_2$ state. The derived transition temperature is $T_{1/2} = \Delta H / \Delta S$ = 392 K.

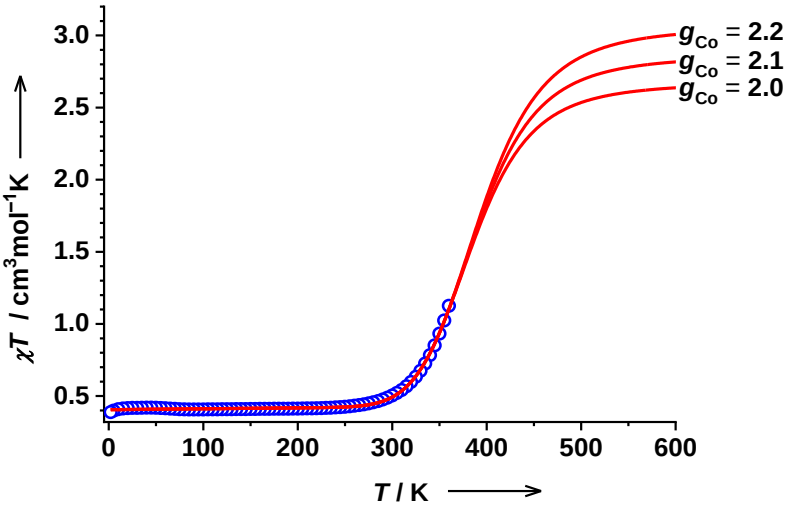

Figure S10: Variable temperature χT product of **1** measured on a powder sample at an external field of 0.1 T in the cooling mode (5 K steps, 2 K min^{-1}). The data has been fitted with differently fixed high temperature limits χT_{HT} according to the given g_{Co} values of the *hs*-Co^{II}(SQ)$_2$ state.

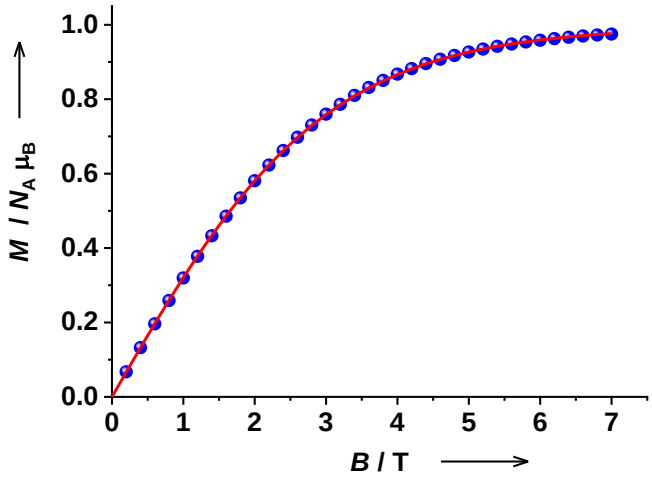

Figure S11: Field-dependent reduced magnetization of **1** measured at temperature T = 2.0 K. Fit parameters: S = 1/2, g = 1.989.

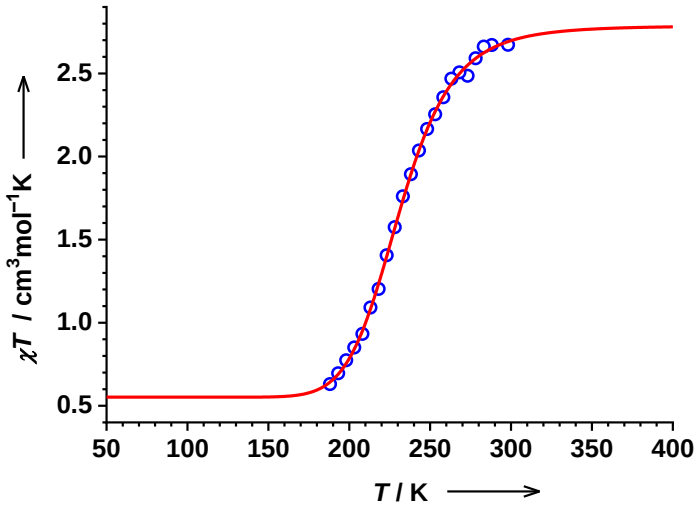

Figure S12: Variable temperature χT product of **1** measured in toluene solution with the Evans NMR method (toluene : toluene-d_8 : TMS = 10 : 2 : 1). Van't Hoff fit parameters: ΔH = 26(2) kJ mol^{-1}, ΔS = 115(9) J mol^{-1} K^{-1}, χT_{LT} = 0.55(2) cm^3 mol^{-1} K, and χT_{HT} = 2.79(3) cm^3 mol^{-1} K. The derived transition temperature is $T_{1/2} = \Delta H / \Delta S$ = 231 K.

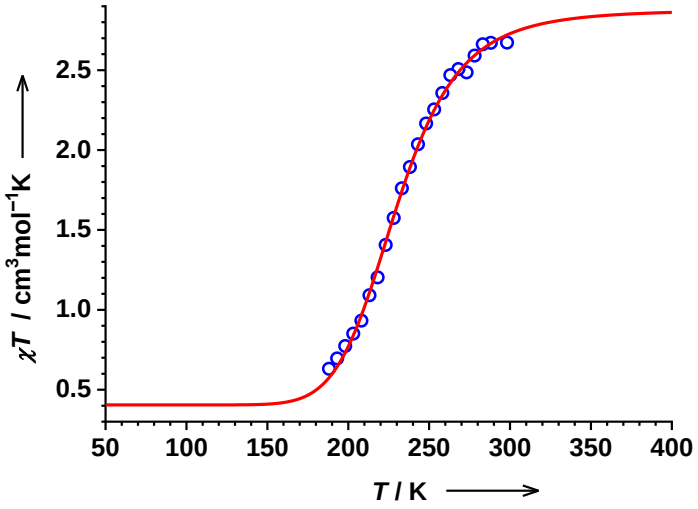

Figure S13: Variable temperature χT product of **1** measured in toluene solution with the Evans NMR method (toluene : toluene-d_8 : TMS = 10 : 2 : 1). Van't Hoff fit parameters: ΔH = 22(1) kJ mol^{-1}, ΔS = 95(5) J mol^{-1} K^{-1}, and χT_{HT} = 2.92(2) cm^3 mol^{-1} K. The low temperature limit χT_{LT} is taken from solid state magnetic measurements and fixed at 0.405 cm^3 mol^{-1} K. The derived transition temperature is $T_{1/2} = \Delta H / \Delta S$ = 230 K.

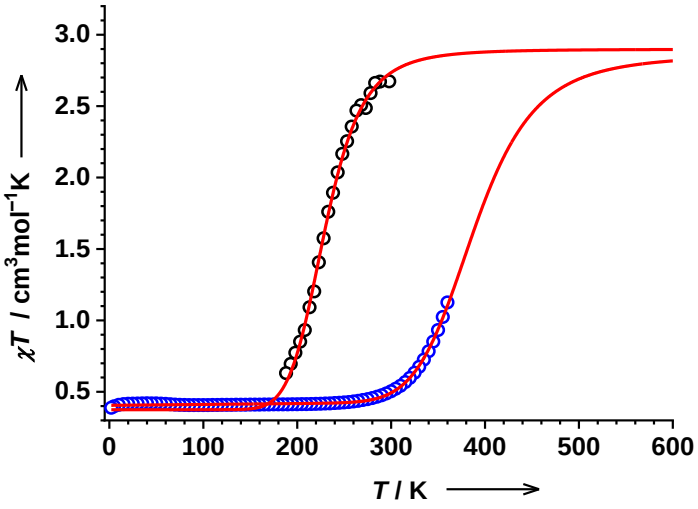

Figure S14: Variable temperature χT product of **1** measured on a powder sample (blue circles, see Fig 2 for details) and variable temperature χT product of **1** measured in toluene solution (black circles, see Fig 3 for details). Van't Hoff fit parameters are compared in **Table S3**.

Table S3: Van't Hoff fit parameters for variable temperature χT product of **1** measured on a powder sample (see Fig 2 and S14) and variable temperature χT product of **1** measured in toluene solution (see Fig 3 and S14).

	$\chi T_{(HT)}$	$\chi T_{(LT)}$	ΔH	ΔS	TIP	$T_{1/2}$
	[cm³ mol^{-1}K]	[cm³ mol^{-1}K]	[kJ mol^{-1}]	[J mol^{-1}K^{-1}]	[cm³mol^{-1}]	[K]
powder	2.814 (fixed)	0.405(2)	38.7(8)	100(2)	6(1)·10^{-5}	388
solution	2.89(4)	0.375 (fixed)	22(1)	95(5)	–	230

EPR Spectroscopy

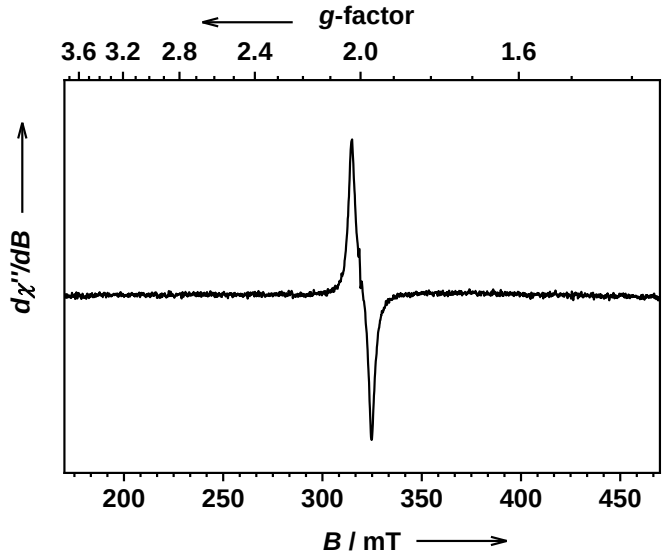

Figure S15: X-band EPR spectrum of **1** in DCM solution (*c* = 10 mM) recorded at 293 K (frequency: 8.9349 GHz, modulation: 0.3 mT, power: 4 mW).

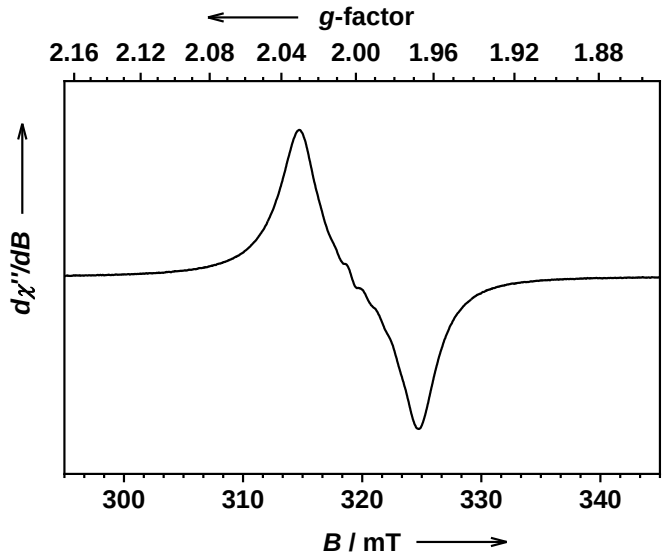

Figure S16: X-band EPR spectrum of **1** in DCM solution (*c* = 10 mM) recorded at 293 K (frequency: 8.9420 GHz, modulation: 0.5 mT, power: 10 mW).

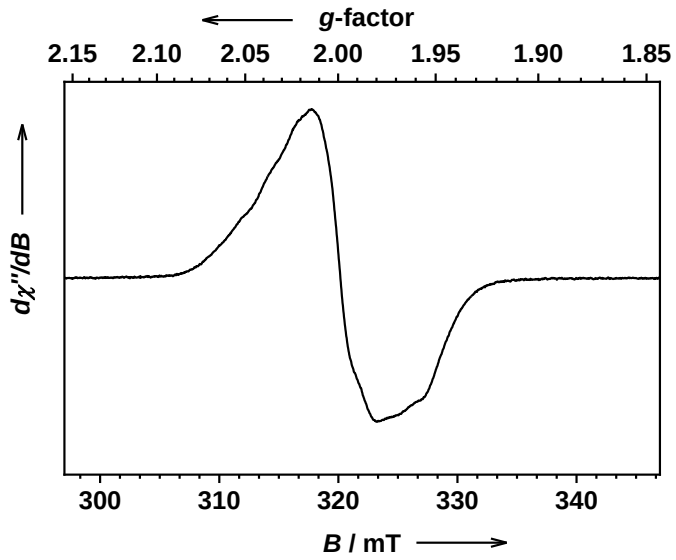

Figure S17: X-band EPR spectrum of **1** in frozen toluene solution (c = 1 mM) recorded at 93 K (frequency: 8.9581 GHz, modulation: 1.0 mT, power: 1 mW).

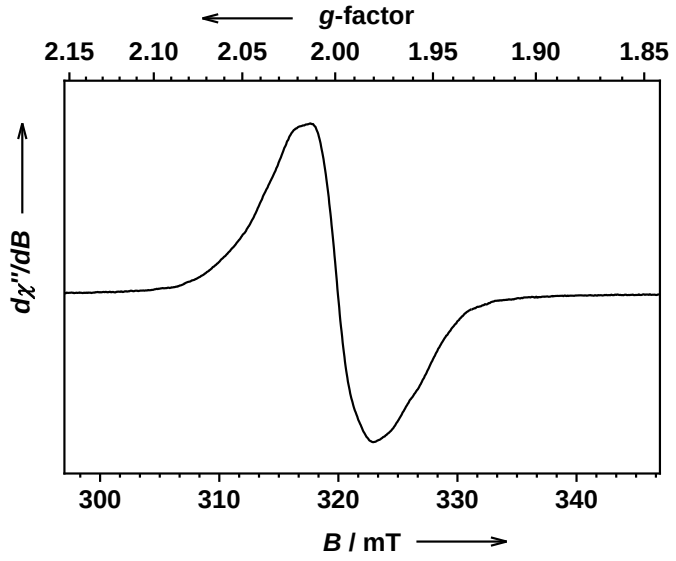

Figure S18: X-band EPR spectrum of **1** in frozen toluene solution (c = 1 mM) recorded at 7 K (frequency: 8.9524 GHz, modulation: 1.0 mT, power: 1 mW).

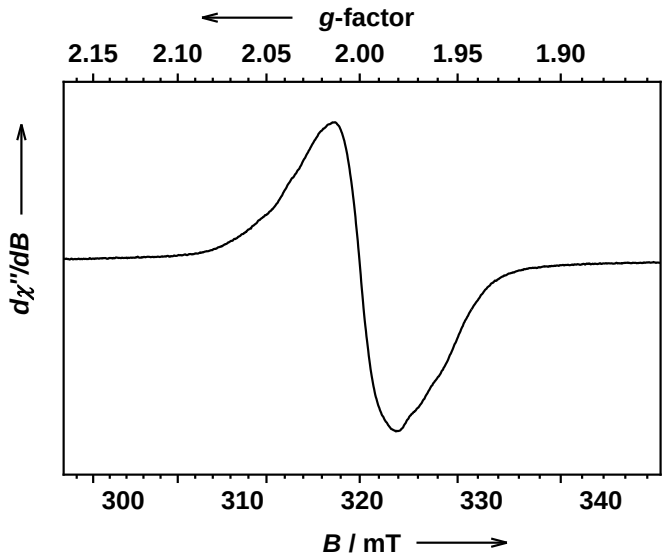

Figure S19: X-band EPR spectrum of **1** in frozen toluene solution (c = 0.1 mM) recorded at 7 K (frequency: 8.9524 GHz, modulation: 0.5 mT, power: 1 mW).

Electronic Absorption Spectroscopy

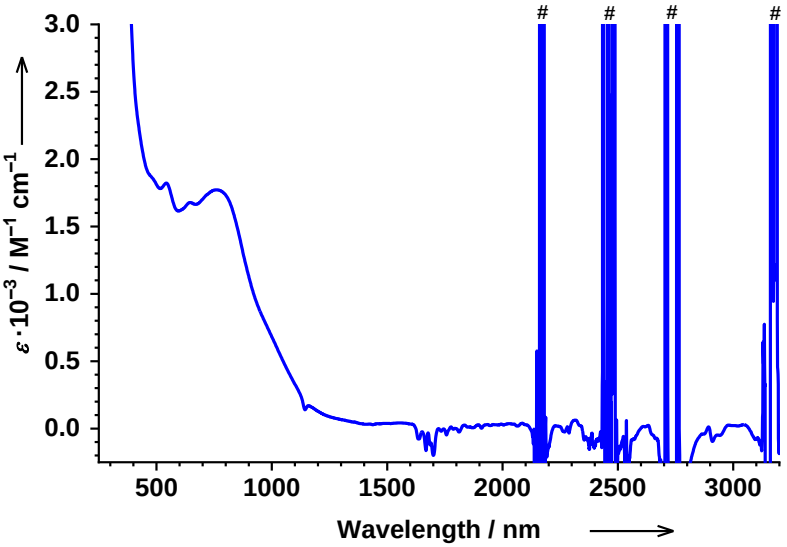

Figure S20: Electronic absorption spectrum of **1** in benzene at room temperature ($c = 5 \cdot 10^{-4}$ M). Negative extinctions due to spectrophotometer artefacts. Artefacts (#) are due to solvent overtones.

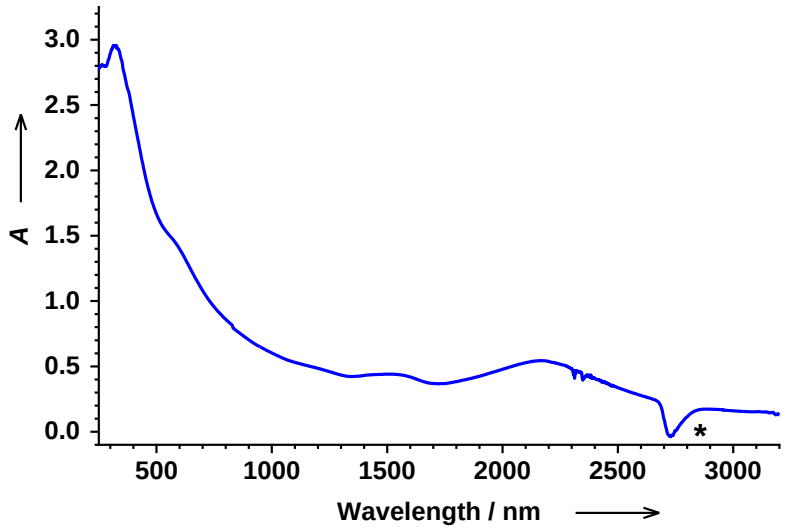

Figure S21: Electronic absorption spectrum of a finely ground solid sample of **1** suspended in Nujol oil. (*) is an artefact.

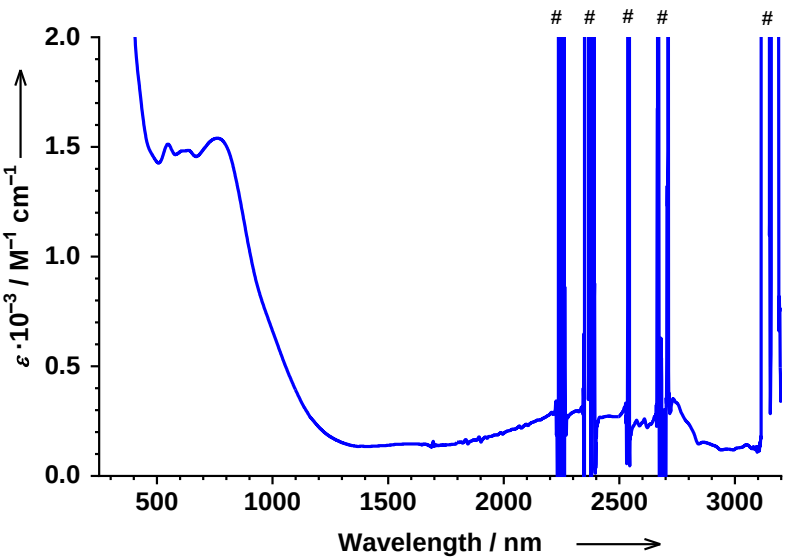

Figure S22: Electronic absorption spectrum of **1** in DCM at room temperature (c = 5·10^{-4} M). Artefacts (#) are due to solvent overtones.

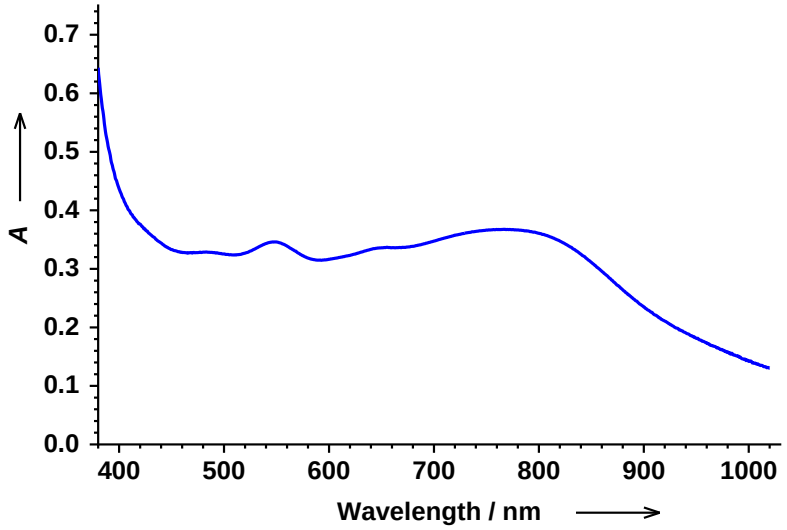

Figure S23: Electronic absorption spectrum of **1** in benzene at room temperature (c = 1.67·10^{-4} M).

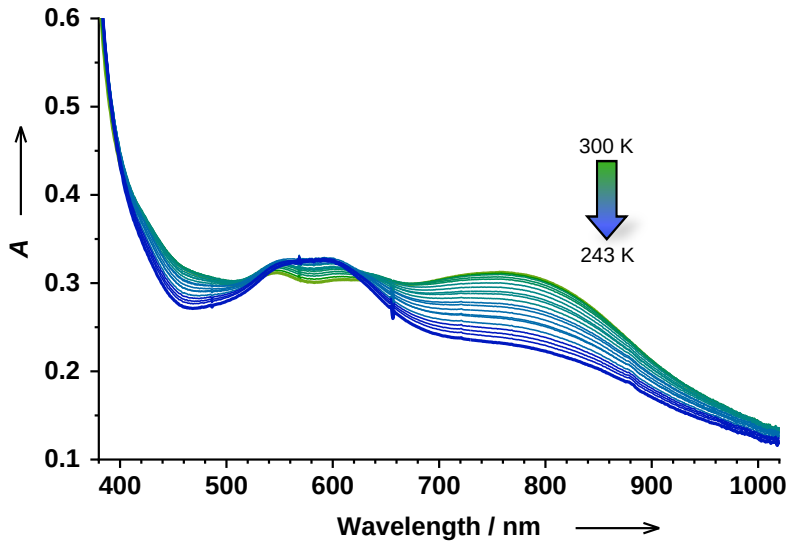

Figure S24: Temperature dependence of the electronic absorption spectrum of **1** in DCM (c = 1.67·10^{-4} M).

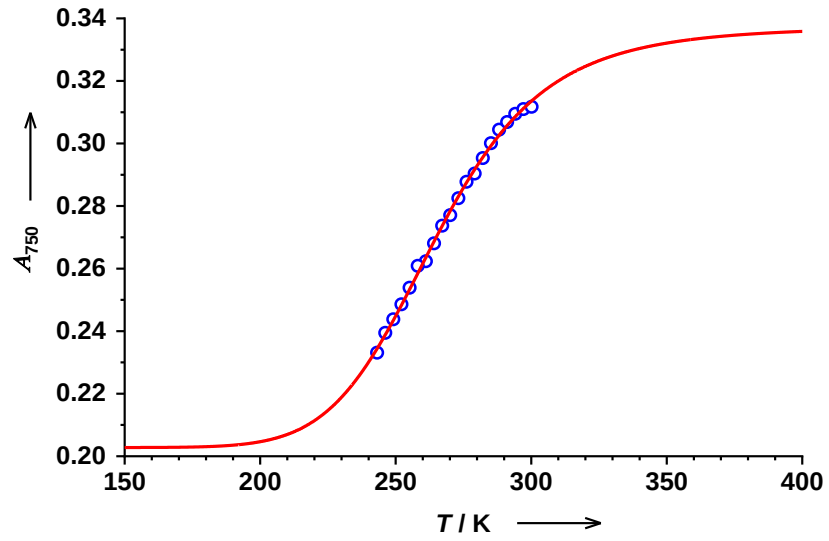

Figure S25: Temperature-dependent evolution of absorption at 750 nm in the electronic absorption spectrum of **1** in DCM (c = 1.67·10^{-4} M). Van't Hoff fit parameters: ΔH = 29(10) kJ mol^{-1}, ΔS = 109(38) J mol^{-1} K^{-1}, A_{LT} = 0.203(1), and A_{HT} = 0.337(1). The derived transition temperature is $T_{1/2} = \Delta H / \Delta S$ = 265 K.

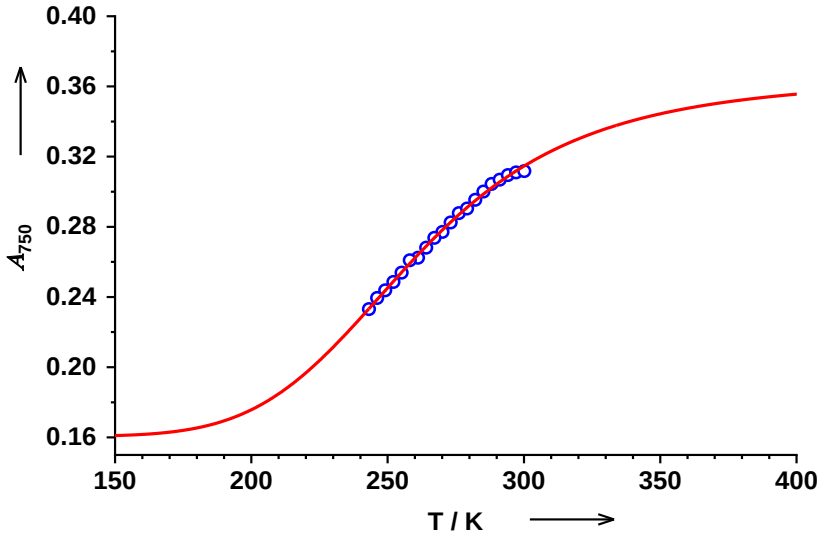

Figure S26: Temperature-dependent evolution of absorption at 750 nm in the electronic absorption spectrum of **1** in DCM (c = 1.67·10^{-4} M). Van't Hoff fit parameters: ΔH = 18(1) kJ mol^{-1}, ΔS = 69(3) J mol^{-1} K^{-1}, and A_{LT} = 0.16(1). The high temperature limit A_{HT} is fixed at 0.366, which is taken from a benzene solution of **1** (c = 1.67·10^{-4} M) recorded at 300 K (see **Figure S23**). The derived transition temperature is $T_{1/2} = \Delta H / \Delta S$ = 261 K.

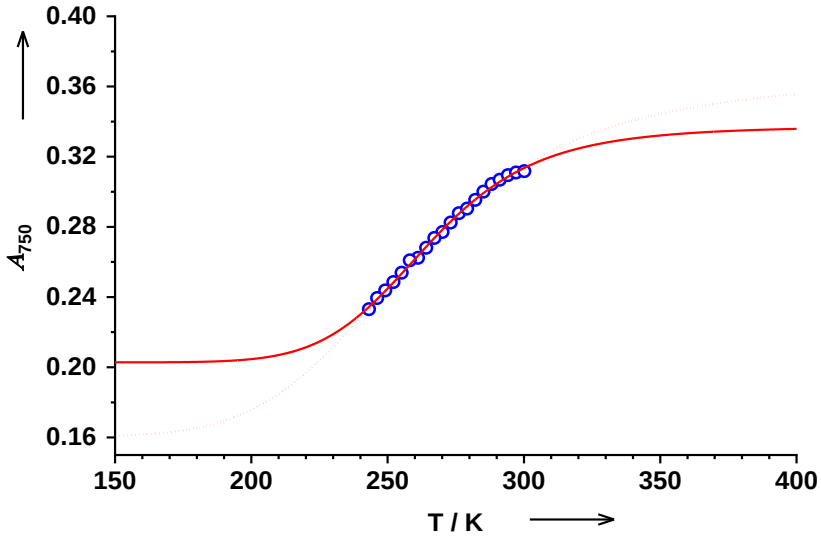

Figure S27: Temperature-dependent evolution of absorption at 750 nm in the electronic absorption spectrum of **1** in DCM (c = 1.67·10^{-4} M). The data has been fitted without any constraints (red line) and with a fixed high temperature limit A_{HT} = 0.366 (red dots).

Cyclic Voltammetry

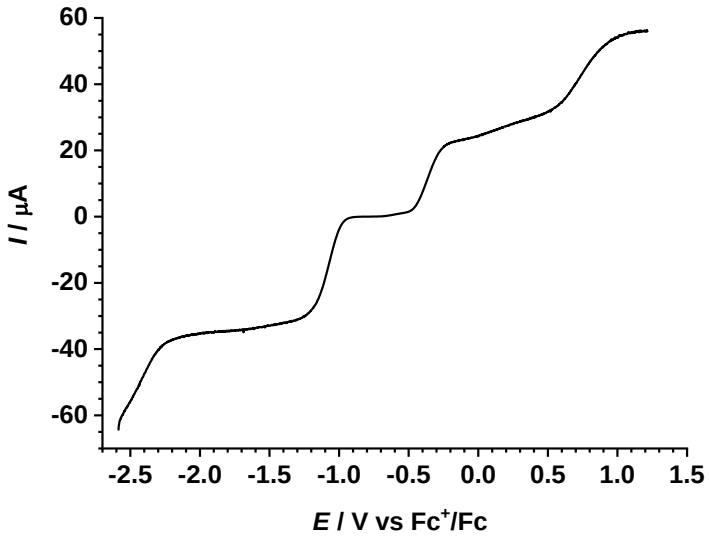

Figure S28: Linear sweep of **1** in DCM solution at RT containing $^{n}Bu_4NPF_6$ (0.1 M) as supporting electrolyte.

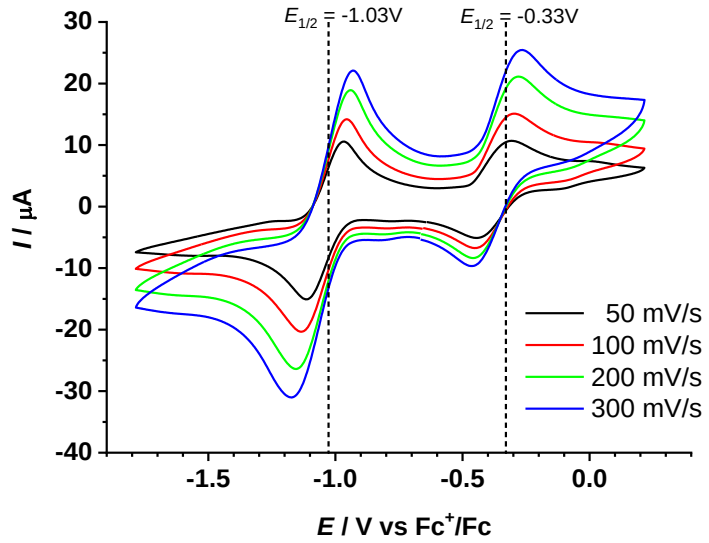

Figure S29: Cyclic voltammogram of **1** in DCM containing $^{n}Bu_4NPF_6$ (0.1 M) as supporting electrolyte, measured at RT and at different scan rates (0.05–0.3 V/s).

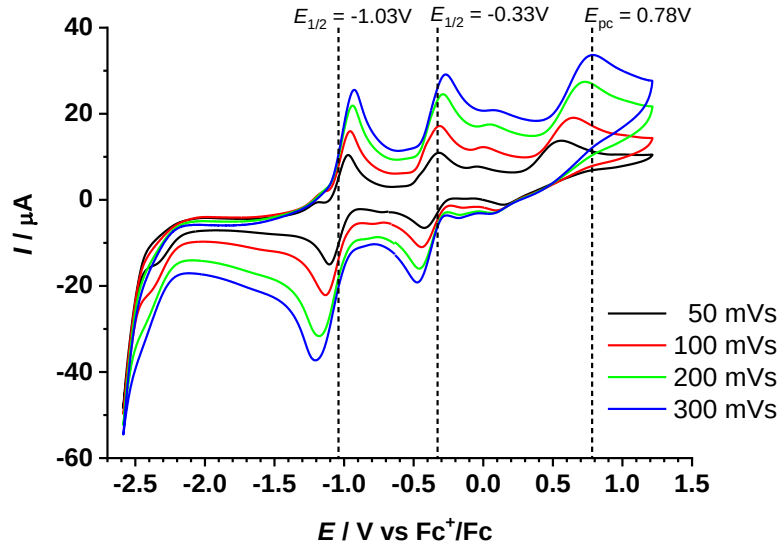

Figure S30: Cyclic voltammogram of **1** in DCM containing $^{n}Bu_4NPF_6$ (0.1 M) as supporting electrolyte, measured at RT and at different scan rates (0.05–0.3 V/s).

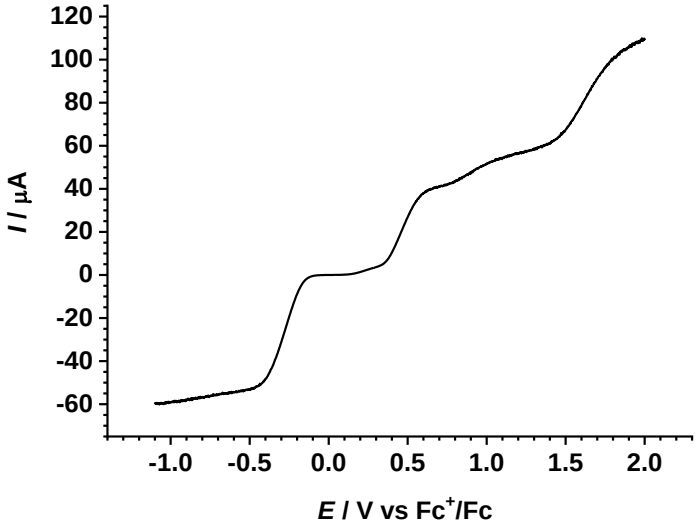

Figure 31: Linear sweep of reference [Co(^{t}Bu-dioxolene)$_2$(phen)] in DCM solution at RT containing $^{n}Bu_4NPF_6$ (0.1 M) as supporting electrolyte.

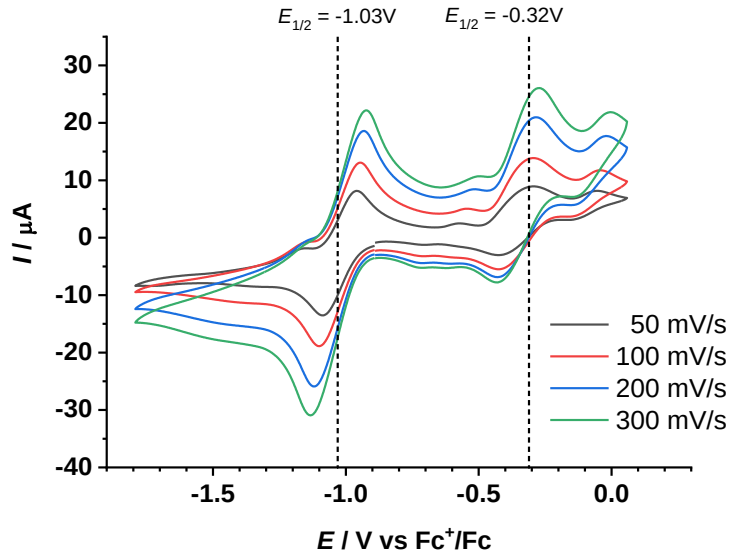

Figure S32: Cyclic voltammogram of reference [Co(^{t}Bu-dioxolene)$_2$(phen)] in DCM containing ^{n}Bu$_4$NPF$_6$ (0.1 M) as supporting electrolyte, measured at RT and at different scan rates (0.05–0.3 V/s).

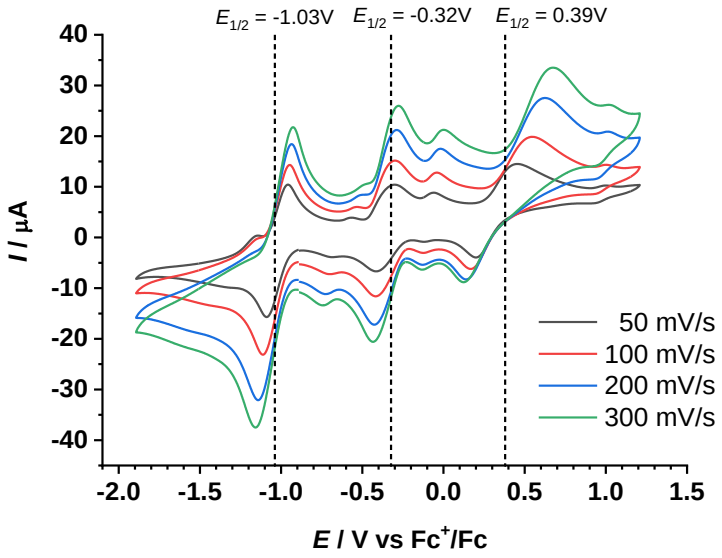

Figure S33: Cyclic voltammogram of reference [Co(^{t}Bu-dioxolene)$_2$(phen)] in DCM containing ^{n}Bu$_4$NPF$_6$ (0.1 M) as supporting electrolyte, measured at RT and at different scan rates (0.05–0.3 V/s).

Table S4: Comparison of electrochemical data (*E*, V) for [Co(^{t}Bu-dioxolene)$_2$(**L**)] (**1**) and three similar complexes with different ligands (**phen** = 1,10-phenanthroline, **papy** = 4-phenylazopyridine, **stypy** = 4-styrylpyridine; tbdiox = ^{t}Bu-dioxolene). Potentials are referenced in DCM *vs* $[Fe(Cp)_2]^+/[Fe(Cp)_2]$.

	[Co(^{t}Bu-dioxolene)$_2$(**L**)](**1**)	[Co(^{t}Bu-dioxolene)$_2$(**stypy**)$_2$][18]	[Co(^{t}Bu-dioxolene)$_2$(**papy**)$_2$][19]	[Co(^{t}Bu-dioxolene)$_2$(**phen**)]
Oxidation	+0.78[#]	+0.7[#]	+0.7[#]	+0.39
Oxidation	–0.33	–0.33	–0.27	–0.32
Reduction	–	–0.67	–0.60	–
Reduction	–1.03	–1.12	–1.13	–1.03
Reduction	–	–	–1.62*	–

[#]*cathodic peak potential for irreversible processes.*

**similar to free 4-papy.*

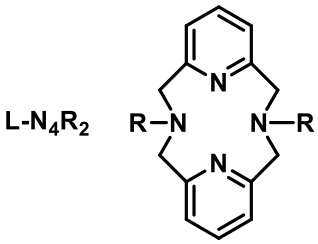

S1: [Co(III)(L-N_4Me_2)(Cat)](BPh_4)
S2: [Co(III)(L-N_4Et_2)(Cat)](BPh_4)
S3: [Co(III)(L-N_4*i*Pr_2)(Cat)](BPh_4)
S4: [Co(II)(L-N_4*t*Bu_2)(SQ)](B(*p*-PhCl)$_4$)
S5: [Fe(III)(L-N_4*i*Pr_2)(Cat)](BPh_4)
S6: [Mn(III)(L-N_4*i*Pr_2)(Cat)](BPh_4)

Scheme S1: Tetraazamacrocyclic ligand and family of complexes **S1**–**S6** used for comparison of electrochemical data.

Table S5: Comparison of electrochemical data (*E*, V) for a family of [(L-N_4R_2)M(^{t}Bu-dioxolene)](BPh_4) complexes (see Scheme S1). Cat^{2-} is the catecholate and $SQ^{\bullet-}$ is the semiquinone redox isomer of ^{t}Bu-dioxolene. The first oxidation and first reduction are shown. Potentials are referenced in MeCN *vs* $[Fe(Cp)_2]^+/[Fe(Cp)_2]$.

	Co(III)-Cat^{2-} **S1**[20]	Co(III)-Cat^{2-} **S2**[21]	Co(III)-Cat^{2-} **S3**[21]	Co(II)-$SQ^{\bullet-}$ **S4**[20]	Mn(III)-Cat^{2-} **S5**[21]	Fe(III)-Cat^{2-} **S6**[21]
Oxidation	–0.11	–0.14	–0.15	–	+0.22	+0.01
Reduction	–*	–1.00	–0.89	–0.80	–0.92	–1.02

**no data for E < –1.0 V is reported.*

Theoretical Calculations

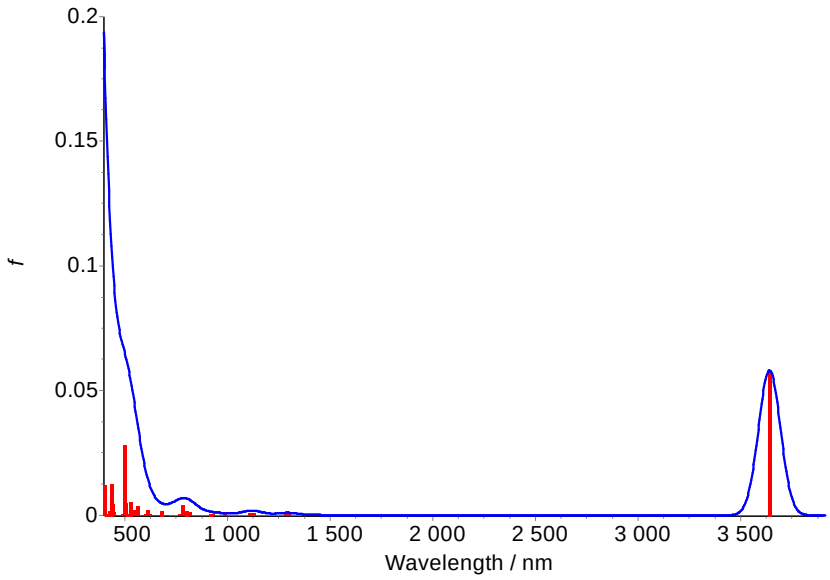

Figure S34: Electronic absorption spectrum of **1** calculated for $S = 1/2$, *i.e.* *ls*-Co(III)(Cat^{2-})($SQ^{\bullet-}$) state with B3LYP-TD-DFT. The LLIVCT band at 3639 nm (2748 cm^{-1}) is to be noticed.

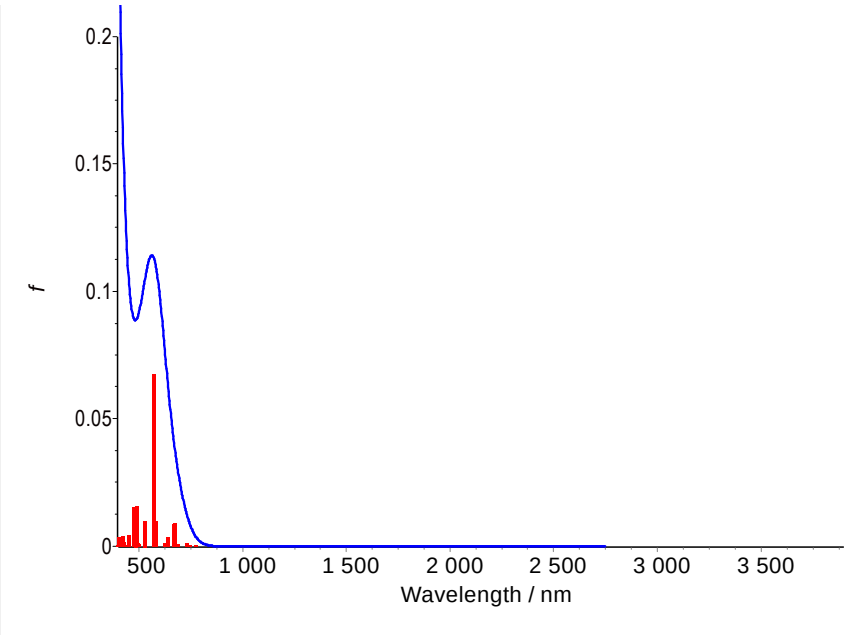

Figure S35: Electronic absorption spectrum of **1** calculated for $S = 5/2$, *i.e.* *hs*-Co(II)($SQ^{\bullet-}$)$_2$ state with B3LYP-TD-DFT. No absorption in NIR or deeper IR regions are expected.

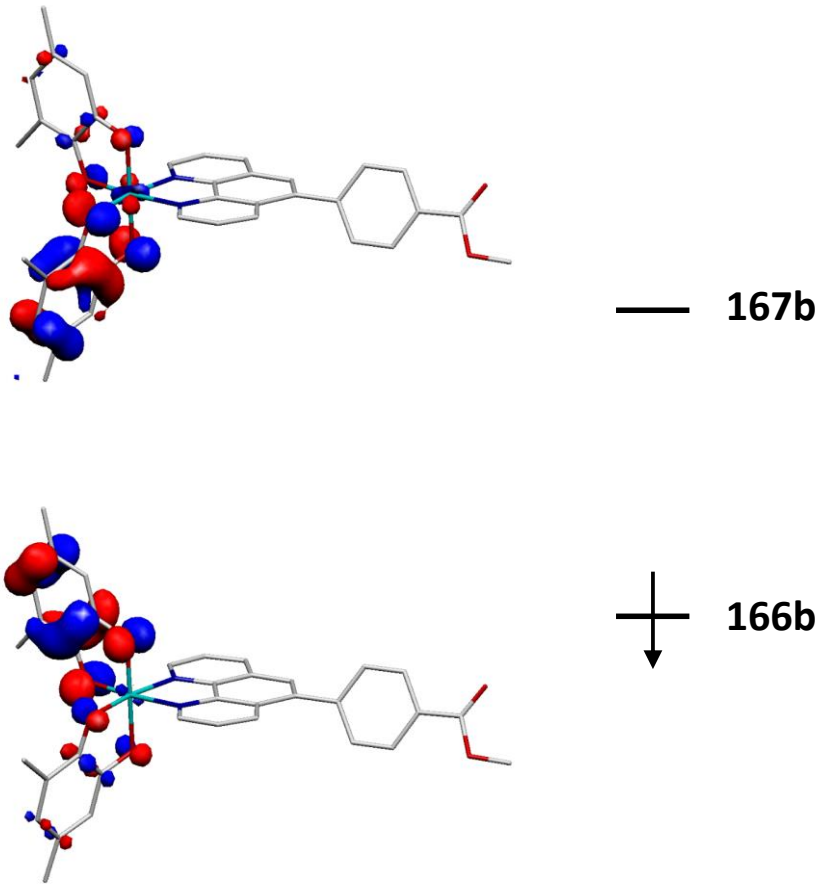

Figure S36: Donor and acceptor molecular orbitals involved into LLIVCT transition calculated at 3639 nm (2748 cm^{-1}) with B3LYP-TD-DFT at *S* = 1/2, *i.e. ls*-Co(III)(Cat^{2-})($SQ^{\bullet-}$) state.

References

1. R. M. Buchanan, B. J. Fitzgerald and C. G. Pierpont, *Inorg. Chem.*, 1979, **18**, 3439-3444.
2. A. Martin, A. Byrne, C. S. Burke, R. J. Forster and T. E. Keyes, *J. Am. Chem. Soc.*, 2014, **136**, 15300-15309.
3. D. M. Adams, A. Dei, A. L. Rheingold and D. N. Hendrickson, *J. Am. Chem. Soc.*, 1993, **115**, 8221-8229.
4. O. Kahn, *Molecular Magnetism*, VCH Publishers Inc., 1993.
5. N. F. Chilton, R. P. Anderson, L. D. Turner, A. Soncini and K. S. Murray, *J. Comput. Chem.*, 2013, **34**, 1164-1175.
6. SADABS 2014/5, Bruker AXS area detector scaling and absorption correction. Bruker AXS, Inc., 2014, Madison WI., USA.
7. G. Sheldrick, *Acta Cryst. A*, 2008, **64**, 112-122.
8. G. Sheldrick, *Acta Cryst. C*, 2015, **71**, 3-8.

9. O. V. Dolomanov, L. J. Bourhis, R. J. Gildea, J. A. K. Howard and H. Puschmann, *J. Appl. Cryst.*, 2009, **42**, 339-341.

10. Neese, F. ORCA 4.1.1 - Ab Initio, DFT and semiempirical electronic structure package. Max-Planck-Institut für Kohlenforschung, Mülheim/Ruhr, Germany

11. C. T. Lee, W. T. Yang and R. G. Parr, *Phys. Rev. B*, 1988, **37**, 785-789.

12. A. D. Becke, *J. Chem. Phys.*, 1993, **98**, 5648-5652.

13. F. Weigend and R. Ahlrichs, *Phys. Chem. Chem. Phys.*, 2005, **7**, 3297-3305.

14. F. Weigend, *Phys. Chem. Chem. Phys.*, 2006, **8**, 1057-1065.

15. V. Barone and M. Cossi, *J. Phys. Chem. A*, 1998, **102**, 1995-2001.

16. Portmann, S. Molekel, version 4.3.win32; CSCS/UNI Geneva, Switzerland, 2002

17. Chemcraft - graphical software for visualization of quantum chemistry computations. https://www.chemcraftprog.com

18. A. Witt, F. W. Heinemann and M. M. Khusniyarov, *Chem. Sci.*, 2015, **6**, 4599-4609.

19. A. Witt, F. W. Heinemann, S. Sproules and M. M. Khusniyarov, *Chem. Eur. J.*, 2014, **20**, 11149-11162.

20. F. Rupp, K. Chevalier, M. Graf, M. Schmitz, H. Kelm, A. Grün, M. Zimmer, M. Gerhards, C. van Wüllen, H.-J. Krüger and R. Diller, *Chem. Eur. J.*, 2017, **23**, 2119-2132.

21. T. Tezgerevska, E. Rousset, R. W. Gable, G. N. L. Jameson, E. C. Sañudo, A. Starikova and C. Boskovic, *Dalton Trans.*, 2019, **48**, 11674-11689.